Revision 1

Non-invasive assessment of the formation of tourmaline nodules by X-ray microtomography and computer modeling

Luca Valentini[1,*], Barbara Marchesini[2], Matteo Parisatto[1], Diego Perugini[2] and Gilberto Artioli[1]

[1]Department of Geosciences, University of Padua, 35128 Padua, Italy.

[2]Department of Physics and Geology, University of Perugia, 06123 Perugia, Italy.

*Email: luca.valentini@unipd.it

ABSTRACT

Tourmaline nodules occurring in the Capo Bianco (Elba Island, Italy) aplitic rocks are here investigated by X-ray microtomography 3D imaging. This non-invasive technique provides 3D images of the tourmaline nodules, revealing an irregular morphology consisting of branches that extend radially from the cores. The nodules present scale-invariant features that can be described by a box-counting fractal dimension. The value of the fractal dimension is proportional to the size of the nodules and tends asymptotically to a value of 2.5, in agreement with the results obtained from the simulation of virtual nodules, by means of a diffusion-limited aggregation model based on a Monte Carlo Metropolis algorithm, in which the growth probability at the tips of the nodule is an inverse function of the diffusion coefficient. The results support the hypothesis that tourmaline formed by a disequilibrium magmatic process, in which diffusion represents the rate-limiting step, inducing the formation of nodules with irregular shapes. This study shows the potential of X-ray microtomography, in combination with numerical modeling, as a probe for accessing the 3D microstructural information of complex mineral morphologies with a non-invasive approach. The combination of numerical and experimental, non-invasive, 3D techniques represents a fundamental step forward in bridging the gap between the observation of microstructures and the interpretation of the associated processes.

Keywords: Disequilibrium, Fractal, Tomography, Tourmaline, Diffusion-limited aggregation

INTRODUCTION

Igneous rocks display a variety of microstructures and compositional heterogeneities that reveal the underlying complexity of the processes associated with their formation. In particular, disequilibrium textures, including skeletal, spherulitic and dendritic morphologies, record the perturbation of the chemical potential within a magmatic system, hence representing geological markers for processes occurring far from equilibrium, due to changes in composition, temperature and pressure (Fowler et al. 1989; Perugini et al. 2003; Jerram and Davidson, 2007). The investigation of the microstructure of igneous rocks is crucial to the understanding of such processes.

Microstructural investigation has traditionally relied on 2D observations based on both optical and electron microscopy (Higgins, 2006). 2D observation may provide overall information on the microstructure of the mineral assemblage, but may potentially lead to erroneous interpretation, since the observed features only contain partial information of the actual 3D microstructure. Another drawback of such methods is their intrinsically invasive nature, since sample preparation requires the destruction of the original 3D microstructure.

An alternative to standard 2D observation is given by serial sectioning or serial grinding, by which vertical sections of a rock sample are sequentially scanned and a virtual 3D image is reconstructed (Byron et al., 1995; Mock and Jerram 2006; Jerram and Higgins 2007). Although such methods have the advantage of accessing the 3D microstructural features, they are affected by some limitations, most notably destructive and time consuming sample preparation, and low spatial resolution (Marschallinger 1998). The spatial resolution of serial imaging methods can be drastically improved by the use of a focused ion beam setup , in combination with electron microscopy and electron backscatter diffraction imaging (Sakamoto et al., 1998; Dunn and Hull, 1999; Inkson et al., 2001; Groeber et al., 2006; Zaafarani et al., 2006).

In recent years, a significant improvement in the 3D microstructural investigation has been achieved by the use of X-ray computed microtomography (X-μCT) analysis (e.g. Carlson, 2006) by means of both conventional and synchrotron X-ray sources. X-μCT is based on the use of mathematical algorithms to reconstruct the internal 3D microstructure of a sample, from a set of 2D projections that record the X-ray attenuation signal, acquired at different angular positions during the rotation of the sample around a vertical axis. X-μCT has been successfully applied to the study of, e.g. the 3D distribution and shape of vesicles in volcanic rocks (Song et al. 2001, Voltolini et al. 2011, Baker et al. 2012) , microstructural analysis of ore-bearing rocks (Godel 2013), 3D characterization of porphyroblasts (Carlson and Denison, 1992; Huddlestone-Holmes and Ketcham 2005, Huddlestone-Holmes and Ketcham 2010) and 3D spatial distribution of the phase assemblage present in cement materials (Artioli et al. 2012).

In this study, X-μCT is used to quantitatively assess the 3D morphology of tourmaline nodules occurring in the aplitic rocks of Capo Bianco (Elba Island, Italy). This study represents an extension to the third dimension of a previous morphological investigation, based on the 2D characterization of the Capo Bianco tourmaline nodules from polished sections of the host rocks, imaged by a high-resolution optical scanner (Perugini and Poli, 2007). In this previous study, the growth pattern of the nodules, quantitatively analyzed by means of fractal geometry, had been associated to a process of non-equilibrium crystallization, in which slow chemical diffusion represents the rate limiting factor to mineral growth.

Here, 3D images of the tourmaline nodules are reconstructed and their morphology is quantified by measuring the associated fractal dimension. The value of the fractal dimension is compared to that of virtual nodules, simulated by a 3D diffusion-limited aggregation (DLA) algorithm, which models the formation of tourmaline in a far-from-equilibrium environment.

ANALYTICAL METHODS

Sample description and preparation

The investigated samples were collected in the Capo Bianco aplite outcrop, in central Elba Island (Tyrrhenian Sea, Italy). The outcrop consists of a tabular intrusive body, with a Rb-Sr age of 7.91 ± 0.1 Ma, having an alkali feldspar granite composition (Dini et al. 2002; see Table 1 for whole rock composition). Dark blue tourmaline nodules having a schorl-elbaite solid solution composition (Dini et al. 2006) are aligned along flow banding structures within the white micro-granitoid host (Perugini and Poli, 2007). A macroscopic inspection of the hand specimens reveals a distribution of sub-centimeter to sub-millimeter sized tourmaline nodules, characterized by a variety of morphologies, from approximately rounded to highly irregular, consisting of a series of branches propagating from the center of the nodules (Fig. 1). Cylindrical cores, having a diameter of 4 mm and height of 15 mm, were drilled from the samples. The size of the cores was selected such that the samples enclosed at least one entire nodule, but were small enough to perform the X-μCT measurements with sufficiently high spatial resolution and optimal compositional contrast.

X-ray microtomography

X-ray tomographic scans were performed at the Department of Geosciences (University of Padua) using a Skyscan 1172 high-resolution X-μCT scanner (Bruker). The cylindrical samples were irradiated by a polychromatic X-ray cone beam, filtered by a 0.5 mm aluminum foil. The X-ray source, equipped with a tungsten anode, operated at an accelerating voltage of 59 kV and a current of 167 μA. The selected experimental setup ensured an appropriate tradeoff between X-ray transmission and absorption contrast. For each sample, 1800 radiographs (Fig. 2a) were acquired over a rotation of 360° with a step of 0.2° and an exposure time of 950 ms for each projection. Three-dimensional assemblages of cross-sectional slices, consisting of 332 to 517 vertically stacked digital images, were obtained by tomographic reconstruction, using a filtered back-projection algorithm (Kak and Slaney 2001). The reconstructed images have a voxel size of 3.4 μm/voxel and consist of maps of the local X-ray attenuation. Since attenuation is in general a function of density and mean atomic number, tomographic imaging allows the mapping of density and composition heterogeneities within a matrix. Typically, grey-scale values are proportional to X-ray absorption, with darker grey colors corresponding to low-attenuation phases and brighter grey colors corresponding to high-attenuation ones. In the specific case of the studied samples, cross sectional slices of the tourmaline nodules (characterized by higher X-ray attenuation) are clearly distinguished within the aplitic, darker matrix (Fig. 2b).

Image processing and analysis

Quantitative analysis of the tourmaline nodules was performed after selecting a series of volumes within the whole 3D stacks. Each cropped volume contains one tourmaline nodule (Fig. 2c). A set of 17 nodules were selected for the image analysis. Conversion from grey-scale to binary images (Fig. 2d) was performed using an iterative selection thresholding algorithm (Riedler and Calvard, 1978) as implemented in the imaging software Image J v1.47 (Schneider et al. 2012). The obtained 3D binary images were then processed by a method based on a union-find algorithm (Sedgewick, 1998) that performs a scan of all the three-dimensionally connected objects within the volume and counts the number of voxels that compose each object. The algorithm keeps the largest object and erases all the others. This procedure removes all the foreign objects that surround the main tourmaline nodule (Fig. 2e). The obtained 3D volumes (Fig. 3) were then analyzed by a box-counting algorithm (Addison, 1997) that calculates their fractal dimension. Mineral phases grown in disequilibrium conditions frequently display scale-invariant features, which can be appropriately described by the principles of fractal geometry (Fowler 1990, Perugini et al. 2003, Perugini et al. 2005). The box-counting fractal dimension D_B is given by the relation:

$$D_B = \lim_{\delta \to 0} \frac{\log(N(\delta))}{\log(1/\delta)} \quad (1)$$

where N is the number of cubes of size δ needed to enclose the volume of the analyzed nodule.

The fractal dimension was used as a quantitative descriptor of the nodules 3D growth pattern. In general, the value of D_B associated with a given object is proportional to the amount of space filled by the object. In the 3D space, a cube has a box counting dimension of 3, whereas a parallelepiped of infinitesimal thickness has a D_B value of 2, because the available space is filled only along two directions. Values of the box-counting dimensions intermediate between 2 and 3 correspond to shapes that fill the 3D space proportionally to D_B and are hence characterized by different degrees of irregularity of their shapes.

Computer model

The growth of the tourmaline nodules is simulated by a 3D diffusion-limited aggregation (DLA) algorithm. DLA essentially consists of a process by which fractal clusters are formed by the diffusive transport of particles throughout the system and their collision and eventual aggregation. In the context of DLA, diffusion is referred to as the random movement of particles (ions, molecules, colloidal particles) driven by thermal energy, rather than the transport down a concentration gradient, which represents a macroscopic phenomenological description of diffusion. Diffusive motion is controlled by the ratio $D = kT/f$ where D is the diffusion coefficient, k is the Boltzmann constant, T is temperature in Kelvin and f is the particle friction, which in the case of a spherical particle of radius R moving in a Newtonian fluid with viscosity μ, is given by $f = 6\pi\mu R$. The magnitude of the diffusive motion is then a direct function of temperature and inverse function of particle size.

The DLA model can then be taken as representative of those processes in which small enough particles (normally of size up to about 1 μm) undergo a random walk, driven by thermal energy, with a rate of diffusion being small compared to the rate at which aggregation occurs.

The DLA algorithm was first introduced to simulate the dendritic growth pattern of metals in 2D (Witten and Sander, 1981; Witten and Sander 1983) and has been extensively applied to the simulation of a variety of processes, including the formation of manganese oxide dendrites in limestone (Chopard et al., 1991; Bayirli and Kockar, 2010), the development of spinifex and harrisitic textures in komatiitic rocks (Fowler et al. 1989, Thériault and Fowler 1995), the kinetics of kaolinite aggregation (Berka and Rice, 2005) and the colloidal aggregation of Au-Ag ores (Saunders and Schoenly, 1995). A 2D version of the algorithm has been previously used to simulate the growth of the Capo Bianco tourmaline nodules (Perugini and Poli, 2007). Here, the process is simulated in 3D and the fractal dimension of the growing DLA cluster is compared to that of the tourmaline nodules imaged by X-μCT.

In the original DLA formulation, a seed particle is placed at the center of the 3D domain and a new particle is released at a given distance and diffuses throughout the 3D space until it comes into contact with the seed and sticks to it to form a cluster. New particles are released sequentially and their diffusive motion is simulated by a random walk algorithm. For each particle, the starting location is selected at a random angular position along a circle with radius $R(i) = r(i) + r_0$, where $r(i)$ is the radius of the growing DLA cluster at the *i*-th iteration and r_0 is a fixed distance. The particles can diffuse to any of the six nearest neighbors, with the direction of motion selected, at any iteration, by casting a random number from a uniform distribution. Each direction of motion is assigned equal probability. When at least one particle of the growing cluster is present in any of the six adjacent voxels, the diffusing particle stops its motion, sticking to the cluster, and a new particle is released. This formulation of the DLA process represents an ideal case in which an infinite dilution of particles in solution is assumed. A more realistic scenario is represented by a system with a finite concentration of particles that diffuse simultaneously (Witten and Meakin, 1983; Fowler et al., 1989). A further variation to the original DLA algorithm is obtained by allowing the particles to aggregate, upon collision with the growing cluster, with a given "sticking probability" p. In the previous study of tourmaline nodule formation by 2D DLA (Perugini and Poli, 2007), the value of p had been empirically related to local physical properties such as surface tension, latent heat of crystallization and curvature of the solid-liquid interface, assuming a variation of a factor 30 of the latent heat of crystallization, due to different regimes in magma convection dynamics. However, given the uncertainty of the absolute values to be assigned to such physical parameters, an alternative method of constraining the probability of particle aggregation, based on a Metropolis Monte Carlo approach (Metropolis et al., 1953), is used in the present study. The transition probability W from one state to a different state of the system, based on the Metropolis algorithm, equals 1 if $\Delta E \leq 0$ (with ΔE being the difference in energy between the final and initial state) whereas if $\Delta E > 0$ it is given by:

$$W = e^{-\frac{\Delta E}{NkT}} \quad (2)$$

where N is the Avogadro constant. If ΔE is chosen as the binding energy of a particle in contact with a growing cluster and it is assumed that the magnitude of the interaction varies linearly with the number n of particle nearest neighbors belonging to the cluster, then the sticking probability can be expressed as:

$$p = 1 - e^{-n\frac{\Delta E}{NkT}} \quad (3)$$

Based on the above equation, the probability that a diffusing particle aggregates to a growing cluster varies proportionally to the total binding energy $n\Delta E$ and to the inverse of the thermal energy kT, which is in turn proportional to the particle diffusivity. Therefore, a process in which diffusion represents the rate-limiting factor is characterized by a large value of p, which drives the system towards the development of irregular, branched morphologies.

In the present study, the computational domain consisted of a mesh of 200 x 200 x 200 lattice sites, with enforced periodic boundary conditions. DLA simulations were performed for both the infinite-dilution and finite-concentration cases, with particle concentrations (expressed as the number of particles embedded in the computational domain, divided by the domain size) of 0.005, 0.025 and 0.05. A binding energy ΔE = 2 $kJmol^{-1}$, in the range of van der Waals interactions (Tilley, 2013) is assumed. A liquidus temperature of 965 °C is calculated, using the model of Ghiorso and Sack (1995), from the whole-rock composition reported in Table 1. By using these parameters, the value of p varies from 0.18 to 0.69, depending on the number of contacts between the particles and the growing cluster. In addition, all the simulations are repeated with the sticking probability p set to the constant value of 1, as in the original DLA formulation. It is important to remark that the calculated liquidus temperature is not necessarily the one at which the process occurred. However, it is here used as an upper limit, since for T < 965 °C the value of the sticking probability p would be closer to the maximum value of 1. The box counting dimension of the DLA cluster was calculated at regular intervals during growth of the cluster.

RESULTS

The reconstructed 3D images show that the tourmaline nodules are formed by micro-crystalline aggregates characterized by irregular shapes, with branches that extend radially from the center of the nodule (Fig. 3). The volume of the nodules varies from 3 x 10^6 to 2 x 10^8 μm^3. The radius of the sphere having equivalent volume varies from 93 to 349 μm.

The box-counting dimension varies from 2.15 to 2.52 (Table 2). The volume and box-counting dimension of the nodules can be measured with an estimated error or approximately 0.5% upon minor variations of the thresholding value. The fractional value of the box-counting dimension D_B indicates that the tourmaline nodules have a fractal morphology. The maximum observed value of D_B is compatible with the theoretical value of 2.5 for 3D DLA clusters at infinite dilution (Addison 1997). The plot "D_B vs. Volume" displayed in Fig. 4 shows the existence of a clear relationship between the size and the box-counting dimension of the nodules. The smallest nodules have values of D_B less than 2.2, whereas when the volume exceeds a size of approximately 5 x 10^7 μm^3 D_B tends asymptotically to the limiting value of 2.5. It is important to remark that calculating the fractal dimension from 2D sections of the nodule may potentially lead to erroneous interpretations. To clarify the importance of a 3D morphological analysis, Fig. 5 displays the fractal dimension calculated from the stacked 2D slices obtained from the tomographic scan of nodule CB1-2 as a function of the vertical stack position. The value of the fractal dimension for the 2D sections vary from 0.29 to 1.83, with most values being in the range 1.4-1.8, whereas the fractal dimension of the whole 3D nodule is 2.30. Therefore, by means of 2D analysis it is not possible to unequivocally quantify the process associated with the formation of the nodules, since no unique value of the fractal dimension can be assigned.

Examples of nodules generated by the DLA methods described in the previous sectioned are displayed in Fig. 6. The variation of the box-counting dimension associated with the simulated nodules, as a function of size, is displayed in Fig. 7. Qualitatively, the simulated variations of D_B with size present a similar trend compared to the experimental distribution presented in Fig. 4, in which the value of D_B increases proportional to the size, until a D_B value of approximately 2.5 is approached. In the infinite-dilution limiting case, the value of D_B rapidly increases above 2 as the nodule grows up to a size of approximately 10^4 voxels and then increases more slowly up to a value of approximately 2.3 at a size of 10^5 voxels. No significant difference in the variation of D_B is observed when the value of p is changed from 1 to that resulting from Equation (3). Similar trends are obtained for the DLA simulations performed with finite concentrations of particles. For a concentration of 0.05 a D_B value of approximately 2.1 is obtained at the final aggregate size of 4 x 10^4 voxels, independent of the value of

p. At a concentration of 0.025, the value of D_B at the final aggregate size of 2 x 10^5 voxels is 2.48 when p has a constant value of 1 and 2.34 when p is obtained from Equation (3). At a concentration of 0.05 and final aggregate size of 4 x 10^5 voxels, the value of D_B is 2.80 for $p = 1$ and 2.55 for p given by Equation (3). The fact that at relatively high particle concentrations, the value of D_B can attain values as high as 2.80 (compared to the theoretical value of 2.50 for a DLA cluster at infinite dilution) as the size of the nodule increases, is related to the fact that in these conditions the mean diffusive length becomes small compared to the distance among the sites at which the particles can aggregate. In other words, the rate-limiting effect of diffusion becomes smaller and a transition from fractal to non-fractal morphologies occurs. Such a transition had been observed in previous finite-concentration DLA simulations (Fowler et al., 1989).

DISCUSSION

The results described in the previous section support the hypothesis, originally postulated by Perugini and Poli (2007), that the Capo Bianco tourmaline nodules formed by a process compatible with a diffusion-limited aggregation model. Other processes have been suggested in the published literature to explain the formation of tourmaline nodules occurring in locations other than Capo Bianco. To the best of our knowledge, the two main hypotheses on the origin of tourmaline nodules alternative to the one illustrated in this study are: (a) formation by hydrothermal alteration of previously crystallized granitic rocks, by means of pervasive B-rich fluids (Rozendaal and Bruwer, 1995; Burianek and Novak, 2004; Yang and Jiang, 2012); (b) late-stage magmatic crystallization by exsolution of a B-rich fluid from the parent magma (Sinclair and Richardson, 1992; Shewfelt et al., 2005; Balen and Broska, 2011). An exhaustive discussion of such alternative hypotheses is present in the work of Perugini and Poli (2007). Here, it is summarized that hydrothermal replacement is not considered to be a valid mechanism for the formation of the Capo Bianco tourmaline nodules, since there is no evidence for the presence of connected fracture networks that may have allowed the permeation of a hydrothermal fluid. In particular, there is no evidence of any dendritically-arranged micro-fractures that according to Rozendaal and Bruwer (1995) may explain the observed morphologies. Moreover, the alignment of the nodules along flow banding features, such as observed at Capo Bianco, is difficult to reconcile with a post-magmatic formation. The late-stage magmatic formation by exsolution of a B-rich fluid is rejected since any evidence of fluid exsolved at low pressures, such as miarolitic cavities, is lacking. In addition to these considerations, it is stressed here that none of the previous studies have focused on the quantitative description and interpretation of the observed fractal morphologies.

In view of the results obtained from the X-μCT characterization and DLA simulations, and in the absence of any alternative process that may quantitatively describe the formation of the observed morphologies, we deem diffusion-limited aggregation to be a viable mechanism for the formation of the Capo Bianco tourmaline nodules. Specifically, DLA mimics the formation of tourmaline nodules in an undercooled magmatic body, in which the formation of fractal aggregates is favored by fast nucleation and slow diffusivity. Any constraint to the actual nature of the diffusing particles is not straightforward. In the work of Perugini and Poli (2007) the DLA process had been regarded as an actual growth mechanism, with a rate limited by the slow diffusion of chemical species down concentration gradients. This is a valid interpretation of the DLA process, although the explicit 3D simulation of molecular diffusion (particle size < 1 nm) leading to the formation of features having a size of about 100 μm, would require a computational domain of at least 10^{18} lattice sites, which is not feasible computationally. Nonetheless, salient information about diffusion-controlled processes, leading to the formation of scale-invariant morphologies, can be obtained even if the scale of the simulated features is orders of magnitude smaller compared to that of the experimentally observed features (Baker and Freda, 1999).

On the other hand, the size of the tourmaline nodules obtained from the DLA simulations can be gauged to that of the natural samples, by assigning a linear resolution of 6 μm/voxel (similar to the X-ray microtomography voxel size of 3.4 μm) to the computational domain. Fig. 8 displays a comparison between the experimentally observed "D_B vs. size" curve and the one obtained from the DLA simulation with particle concentration of 0.05 and sticking probability expressed by Equation (3), to which a lattice size of 6 μm/voxel is assigned. The figure shows a very good agreement between the experimental and simulated curves. This would require the assumption that, in the DLA simulation, the random walkers represent previously crystallized tourmaline particles, having a size of approximately 6 μm, which move randomly throughout the system, driven by thermal energy, and form aggregates by repeated collisions. Further research and more advanced computational models might clarify the exact nature of the diffusing species present in the DLA process.

IMPLICATIONS

The tourmaline nodules occurring in the Capo Bianco aplitic rocks are an example of mineral phases formed in an environment far from equilibrium, which prevented the formation of fully developed crystal faces and regular shapes. The correct interpretation of disequilibrium textures can shed light on the associated geological processes, which drove the system away from a pre-existing state of equilibrium. In this study, the interpretation of the observed morphologies relies on accessing the 3D micro-structural information with a non-invasive approach, by X-μCT and computer simulations based on a 3D diffusion-limited aggregation model.

The results extend the findings of a previous 2D study (Perugini and Poli, 2007) to a more robust 3D microstructural interpretation, supporting the magmatic origin of the tourmaline nodules, by a disequilibrium process in an undercooled environment, in which diffusion represents the rate-limiting factor, resulting in the growth of irregular, branching shapes. In the simulations presented in this study, the probability of the diffusing particle to aggregate to larger clusters is an inverse function of the factor kT (which is proportional to the diffusion coefficient) and the results suggest that departure from fractal behavior may occur when the diffusive length becomes small compared to the distance among the sites at which the particles can aggregate.

This study also proves the potential of X-ray computed microtomography as a powerful microstructural probe for the non-invasive investigation and assessment of the 3D growth patterns and mechanisms associated with mineral phases forming in a perturbed magmatic environment.

Further advance in microstructural investigation of disequilibrium mineral assemblages may be achieved by methods that combine tomographic 3D imaging with the mineral phase selectivity of X-ray diffraction (Artioli et al. 2010, Valentini et al. 2012, Voltolini et al. 2013). This method allows the reconstruction of 3D phase maps, even for samples consisting of an assemblage of mineral phases characterized by low X-ray attenuation contrast.

The combination of such non-invasive 3D imaging methods with numerical 3D models provides a framework for bridging the gap between microstructural observation and interpretation of the associated geological processes.

ACKNOWLEDGMENTS

Financial support for the X-ray computed micro-tomography laboratory of the Department of Geosciences (University of Padua) was entirely provided by Fondazione Cassa di Risparmio di Padova e Rovigo (CaRiPaRo). The constructive reviews of Marco Voltolini and William Carlson were greatly appreciated and significantly improved the overall quality of the original manuscript. Don Baker is acknowledged for additional comments and editorial handling.

REFERENCES CITED

Addison, P.S. (1997) Fractals and Chaos, an Illustrated Course. Institute of Physics Publishing, London, UK.

Artioli, G., Cerulli, T., Cruciani, G., Dalconi, M.C., Ferrari, G., Parisatto, M., Rack, A., and Tucoulou, R. (2010) X-ray diffraction microtomography (XRD-CT), a novel tool for non-invasive mapping of phase development in cement materials. Analytical and Bioanalytical Chemistry, 397, 2131-2136.

Artioli, G., Dalconi, M.C., Parisatto, M., Valentini, L., Voltolini, M., and Ferrari, G. (2012) 3D imaging of complex materials: the case of cement. International Journal of Materials Research, 103, 145-150.

Baker, D.R., and Freda, C. (1999) Ising models of undercooled binary system crystallization: Comparison with experimental and pegmatite textures. American Mineralogist, 84, 725-732.

Baker, D.R., Mancini, L., Polacci, M., Higgins, M.D., Gualda, G.A.R, Hill, R.J., and Rivers, M.L. (2012) An introduction to the application of X-ray microtomography to the three-dimensional study of igneous rocks. Lithos, 148, 262-276.

Balen, D., and Broska, I. (2011) Tourmaline nodules: products of devolatilization within the final evolutionary stages of granitic melt? In A.N. Sial, Ed., Granite-Related Ore Deposits, p. 53-68, Geological Society of London, U.K.

Bayirli, M., and Kockar, H. (2010) A numeric application using diffusion limited aggregation model for the manganese dendrites. Zeitschrift fur Naturforschung, 65a, 777-780.

Berka, M., and Rice, J.A. (2005) Relation between aggregation kinetics and the structure of kaolinite aggregates. Langmuir, 21, 1223-1229.

Burianek, D., and Novak, M. (2004) Morphological and compositional evolution of tourmaline from nodular granite at Lavicky, near Velke Mezirici, Moldanubicum, Czech Republic. Journal of the Czech Geological Society, 49, 81-90.

Byron, D.N., Atherton, M.P, and Hunter, R.H. (1995) The interpretation of granitic textures from serial thin sectioning, image analysis and three-dimensional reconstruction. Mineralogical Magazine, 59, 203-211.

Carlson, W.D. (2006) Three-dimensional imaging of earth and planetary materials. Earth and Planetary Science Letters, 249, 133-147.

Carlson, W.D., and Denison, C. (1992) Mechanisms of porphyroblasts crystallization : results from high-resolution Computed X-ray Tomography. Science, 257, 1236-1239.

Chopard, B., Herrmann, H.J., and Vicsek, T. (1991) Structure and growth mechanism of mineral dendrites. Nature, 353, 409-412.

Dini, A., Innocenti, F., Rocchi, S., Tonarini, S., and Westerman, D.S. (2002) The magmatic evolution of the late Miocene laccolith–pluton–dyke granitic complex of Elba Island, Italy. Geological Magazine, 139, 257–279.

Dini A, Corretti A, Innocenti F, Rocchi S, and Westerman DS (2006) Sooty sweat stains or tourmaline spots? The Argonauts at Elba Island (Tuscany) and the spread of Greek trading in the Mediterranean Sea. In: Piccardi L et al. Eds., Myth and geology. Geological Society of London Special Publication.

Dunn, D.N., and Hull, R. (1999) Reconstruction of three-dimensional chemistry and geometry using focused ion beam microscopy. Applied Physics Letters, 75, 3414.

Fowler, A.D. (1990) Self-organized mineral textures of igneous rocks: the fractal approach. Earth Science Reviews, 29, 47-55.

Fowler, A.D., Stanley, H.E., and Daccord, G. (1989) Disequilibrium silicate mineral textures: fractal and non-fractal features. Nature, 341, 134-138.

Ghiorso, M.S., and Sack, R.O. (1995) Chemical mass transfer in magmatic processes . IV. A revised and internally consistent thermodynamic model for the interpolation and extrapolation of liquid-solid equilibria in magmatic systems at elevated temperatures and pressures. Contributions to Mineralogy and Petrology, 119, 197-212.

Godel, B. (2013) High-resolution X-ray computed tomography and its application to ore deposits: from data acquisition to quantitative three-dimensional measurements with case studies from Ni-Cu-PGE deposits. Economic Geology, 108, 2005-2019.

Groeber, M.A., Haley, B.K., Uchic, M.D., Dimiduk, D.M., and Ghosh, S. (2006) 3D reconstruction and characterization of polycrystalline microstructures using a FIB–SEM system. Materials Characterization, 57, 259-273.

Higgins, M.D. (2006) Quantitative textural measurements in igneous and metamorphic petrology. Cambridge university press, Cambridge.

Huddlestone-Holmes, C.R., and Ketcham, R.A. (2005) Getting the inside story: using computed X-ray tomography to study inclusion trails in garnet porphyroblasts. American Mineralogist, 90, ea1-ea17.

Huddlestone-Holmes, C.R., and Ketcham, R.A. (2010) An X-ray computed tomography study of inclusion trail orientations in multiple porphyroblasts from a single sample. Tectonophysics, 480, 305-320.

Inkson, B.J., Steer, T., Möbus, G., and Wagner, T. (2001) Subsurface nanoindentation deformation of Cu–Al multilayers mapped in 3D by focused ion beam microscopy. Journal of Microscopy, 201, 256-269.

Jerram, D.A., and Davidson, J.P. (2007) Frontiers in textural and microgeochemical analysis. Elements, 3, 235-238.

Jerram, D.A., and Higgins, M. (2007) 3D Analysis of rock textures: quantifying igneous microstructures. Elements, 3, 239-245.

Kak, A.C., and Slaney, M. (2001) Principles of Computerized Tomographic Imaging, Society of Industrial and Applied Mathematics.

Marschallinger, R. (1998) Correction of geometric errors associated with the 3-D reconstruction of geological materials by precision serial lapping. Mineralogical Magazine, 62, 783, 792.

Metropolis, N., Rosenbluth, A.W., Rosenbluth, M.N., Teller, A.H., Teller, E. (1953) Equation of state calculation by fast computing machines. Journal of Chemical Physics, 21, 1087.

Mock, A., and Jerram, D.A. (2006) Crystal size distribution (CSD) in three dimensions: insights from the 3D reconstruction of a highly porphyritic rhyolite. Journal of Petrology, 46, 1525-1541.

Perugini, D. and Poli, G. (2007) Tourmaline nodules from Capo Bianco aplite (Elba Island, Italy): an example of diffusion limited aggregation growth in a magmatic system. Contributions to Mineralogy and Petrology, 153, 493-508.

Perugini, D., Busà, T., Poli, G., and Nazzareni, S. (2003) The role of chaotic dynamics and flow fields in the development of disequilibrium textures in volcanic rocks. Journal of Petrology, 44, 733-756.

Perugini, D., Poli, G., and Valentini, L. (2005) Strange attractors in plagioclase oscillatory zoning: Petrological implications. Contributions to Mineralogy and Petrology, 149, 482-497.

Riedler, T.W., and Calvard, S. (1978) Picture thresholding using an iterative selection method. IEEE Transactions on Systems, Man and Cybernetics, SMC-8, 630-632.

Rocchi, S., Dini, A., Innocenti, F., Tonarini, S., and Westerman, D.S. (2003) Elba Island: intrusive magmatism. Periodico di Mineralogia, 72, 73-104.

Rozendaal, A., and Bruwer, L. (1995) Torumaline nodules: indicator of hydrothermal alteration ans Sn-Zn-(W) mineralization in the Cape Granite Suite, South Africa. Journal of African Earth Sciences, 21, 141-155.

Sakamoto, T., Cheng, C., Takahashi, M., Owari, M., and Nihei, Y. (1998) Development of an ion and electron dual focused beam apparatus for three-dimensional microanalysis. Japanese Journal of Applied Physics, 37, 2051.

Saunders. J.A., and Schoenly, P.A. (1995) Boiling, colloid nucleation and aggregation, and the genesis of bonanza Au-Ag ores of the Sleeper deposit, Nevada. Mineralium Deposita, 30, 199-210.

Schneider, C.A., Rasband, W.S., and Eliceiri, K.W. (2012) NIH Image to ImageJ: 25 years of image analysis. Nature Methods, 9, 971-675.

Sedgewick, R. (1998) Algorithms in C, 720 p. Addison-Wesley, Boston.

Shefwelt, D., Ansdell, K., and Sheppard, S. (2005) The origin of tourmaline nodules in granites; preliminary findings from the Paleoproterozoic Scrubber Granite. Geological Survey of Western Australia Annual Review, 59-63.

Sinclair, D.W., and Richardson, J.M. (1992) Quartz-tourmaline orbicles in the Seagull Batholith, Yukon Territory. Canadian Mineralogist, 30, 923-935.

Song, S.R., Jones, K.W., Lindquist, B.W., Dowd, B.A., and Sahagian D.L. (2001) Synchrotron X-ray computed microtomography: studies on vesiculated basaltic rocks. Bulletin of Volcanology, 4, 252-263.

Thériault, R.D. and Fowler, A.D. (1995) Harrisitic textures in the Centre Hill complex, Munro Township, Ontario: product of diffusion limited growth. Mineralogy and Petrology, 54, 35-44.

Tilley, R.J.D. (2013) Understanding Solids, 2nd edition, 576 p. John Wiley & Sons, Chichester.

Valentini, L., Artioli, G., Dalconi, M.C., and Voltolini, M. (2012) Multifractal analysis of calcium silicate hydrate (C-S-H) mapped by X-ray diffraction microtomography. Journal of the American Ceramic Society, 95, 2647-2652.

Voltolini, M., Zandomeneghi, D., Mancini, L., and Polacci, M. (2011) Texture analysis of volcanic rock samples: quantitative study of crystals and vesicles shape preferred orientation from X-ray microtomography data. Journal of Volcanology and Geothermal Research, 202, 83-95.

Voltolini, M., Dalconi, M.C., Artioli, G., Parisatto, M., Valentini, L., Russo, V., Bonnin, and Tucoulou, R. (2013) Understanding cement hydration at the microscale: new opportunities from 'pencil-beam' synchrotron X-ray diffraction tomography. Journal of Applied Crystallography, 46, 142-152.

Witten, T.A., and Meakin, P. (1983) Diffusion-limited aggregation at multiple growth sites. Physical Review B, 28, 5632-5642.

Witten , T.A., and Sander L.M. (1981) Diffusion-limited aggregation, a kinetic critical phenomenon. Physical Review Letters, 47, 1400.

— (1983) Diffusion-limited aggregation. Physical Review B, 27, 5686–5697.

Yang, S., and Jiang, S. (2012) Chemical and boron isotopic composition of tourmaline in the Xiangshan volcanic–intrusive complex, Southeast China: Evidence for boron mobilization and infiltration during magmatic–hydrothermal processes. Chemical Geology, 312-313, 177-189.

Zaafarani, N., Raabe, D., Singh, R.N., Roters, F., and Zaeffer, S. (2006) Three-dimensional investigation of the texture and microstructure below a nanoindent in a Cu single crystal using 3D EBSD and crystal plasticity finite element simulations. Acta Materialia, 54, 1863-1876.

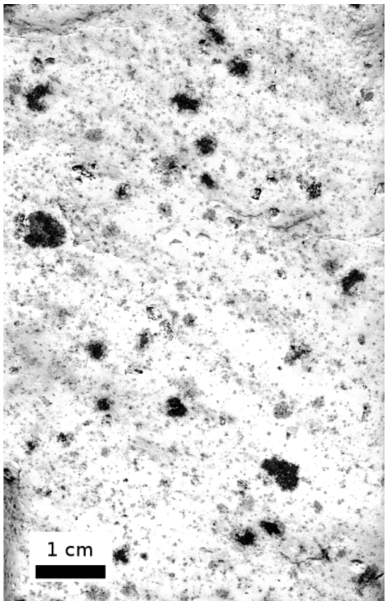

FIGURE 1 Optical scan of a hand specimen displaying the dark tourmaline nodules dispersed in the white aplitic matrix.

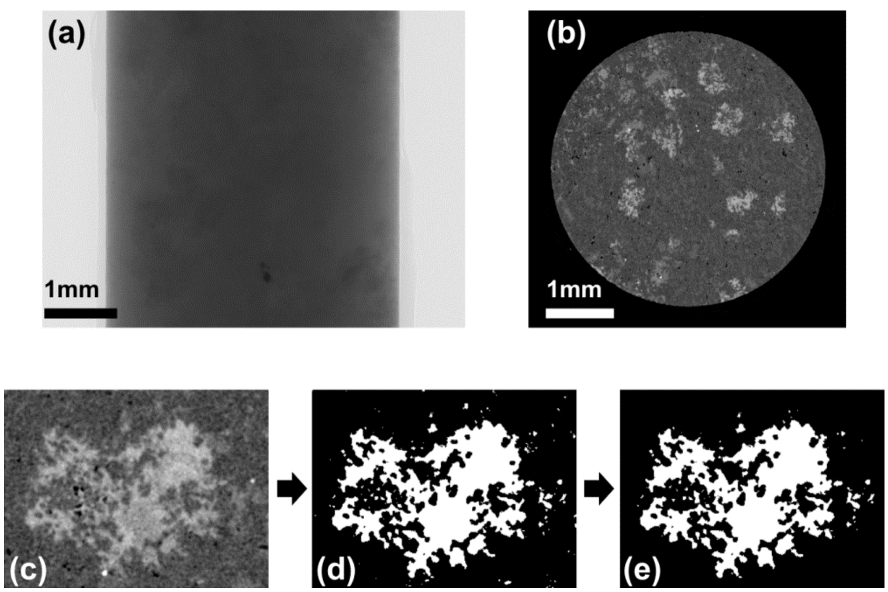

FIGURE 2 Workflow relative to the imaging of the tourmaline nodules: (a) X-ray radiograph of a cylindrical 4 mm-thick sample; (b) reconstructed cross-sectional slice displaying the tourmaline nodules (light gray) dispersed in the aplitic matrix (dark gray); (c) cropped portion of a cross-sectional

slice through a single nodule; (d) thresholded binary image of the nodule (white) surrounded by matrix (black); (e) binary image after 3D removal of the foreign objects surrounding the nodule.

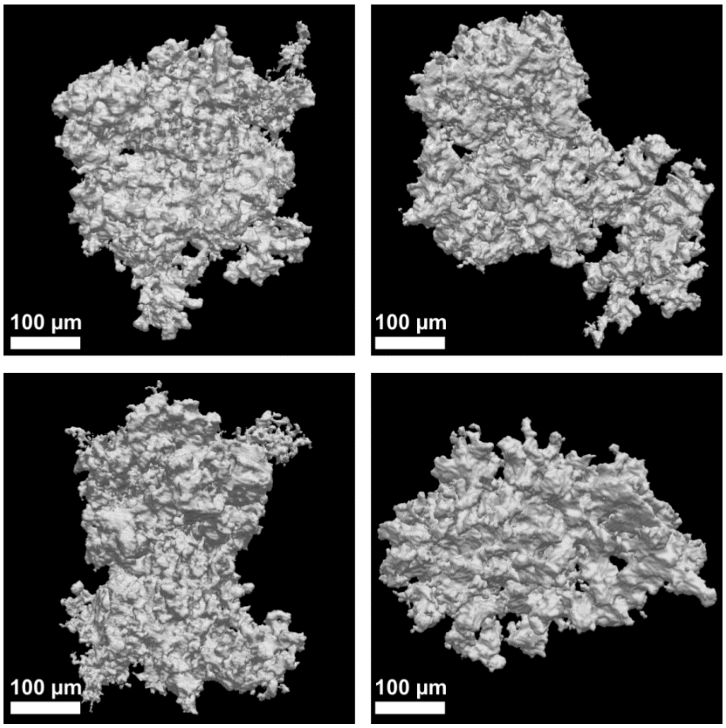

FIGURE 3 Three-dimensional rendering of four tourmaline nodules, obtained from the reconstructed tomographic images.

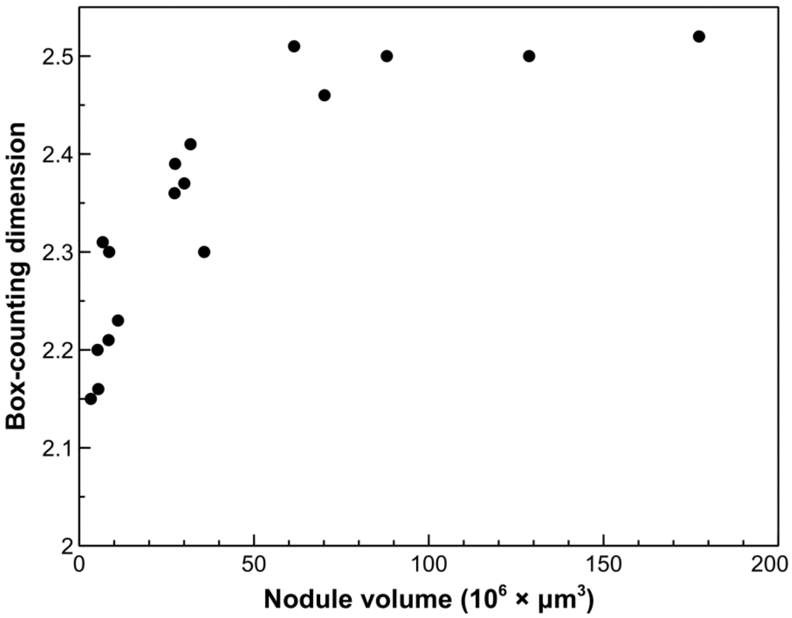

FIGURE 4 Plot of box-counting dimension versus volume for the analyzed tourmaline nodules.

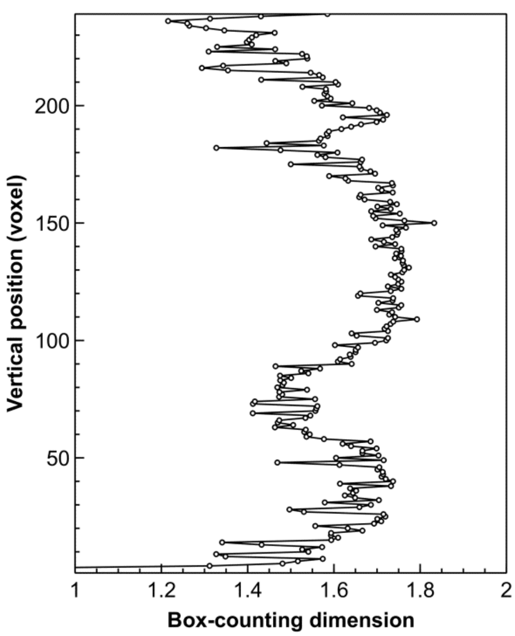

FIGURE 5 Plot of box-counting dimension as a function of the vertical position relative to the stacked 2D slices obtained by X-μCT for nodule CB1-2 .

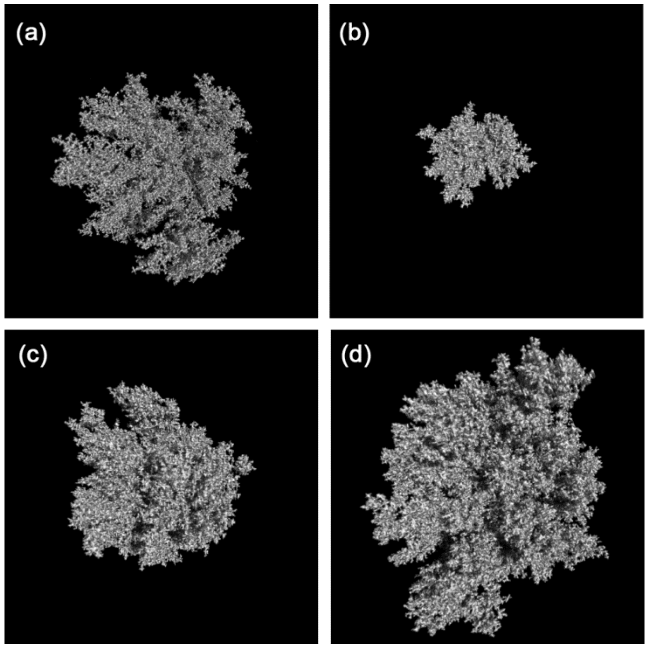

FIGURE 6 Three-dimensional rendering of the virtual nodules obtained by DLA simulations with sticking probabilities calculated from Equation (3): (a) infinite dilusion; (b) 0.005 particle concentration; (c) 0.025 particle concentration; (d) 0.05 particle concentration.

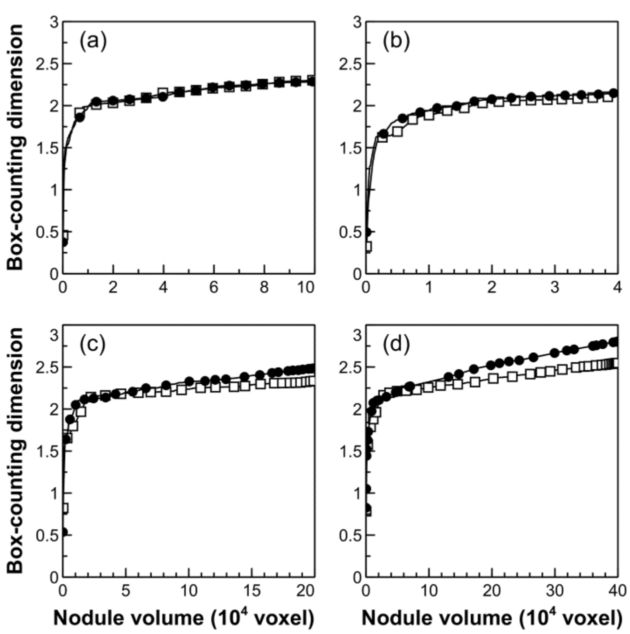

FIGURE 7 Plots of box-counting dimension versus volume for the DLA simulations (black circles: p = 1; white squares: p calculated from Equation 3): (a) infinite dilution; (b) 0.005 particle concentration; (c) 0.025 particle concentration; (d) 0.05 particle concentration.

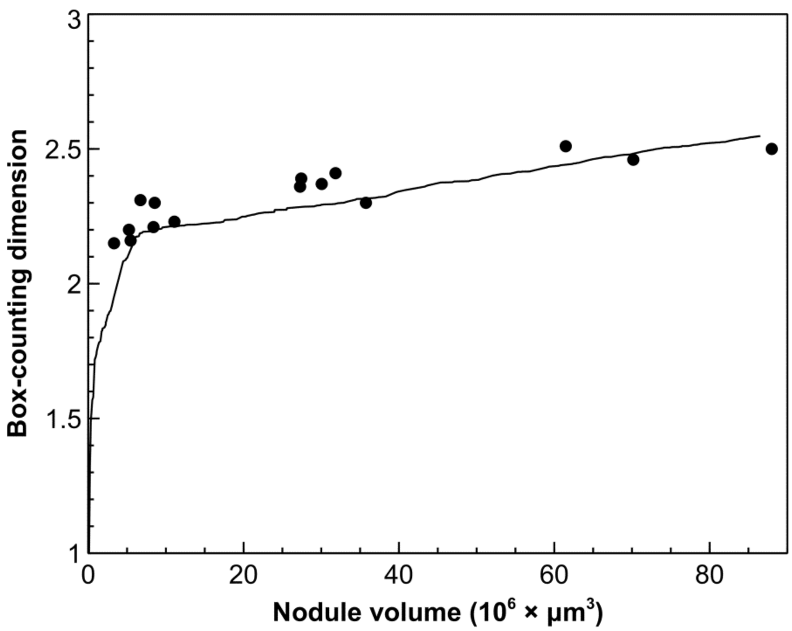

FIGURE 8 Comparison of the "D_B vs. volume" curves for the natural nodules as measured by X-μCT and the nodules simulated by DLA (0.05 particle concentration and p calculated by Equation 3) with a lattice size of 6 μm/voxel.

(DOI will not work until issue is live.) DOI: http://dx.doi.org/10.2138/am-2015-4987 8/20

TABLE 1 Whole rock composition for the Capo Bianco aplite (data from Rocchi et al., 2003)

Element	SiO2	TiO2	Al2O3	Fe2O3	FeO	MnO	MgO	CaO	Na2O	K2O	P2O5	LOI
Wt. %	73.07 (66)	0.02 (1)	16.59 (57)	0.23 (11)	0.23 (8)	0.05 (3)	0.09 (7)	0.22 (14)	4.24 (35)	4.06 (10)	0.02 (1)	1.26 (8)

TABLE 2 Volume and box-counting dimension associated with the measured tourmaline nodules

Nodule	Volume (10^6 x μm^3)	Box-counting dimension
CB1-1	61.48	2.51
CB1-2	35.75	2.30
CB1-3	27.27	2.36
CB1-4	31.84	2.41
CB1-5	30.06	2.37
CB1-6	88.00	2.50
CB1-7	70.17	2.46
CB1-8	8.56	2.30
CB2-10	177.33	2.52
CB2-11	5.24	2.20
CB2-12	6.72	2.31
CB2-13	3.33	2.15
CB2-14	5.46	2.16
CB2-15	11.09	2.23
CB2-16	27.42	2.39
CB2-17	8.40	2.21
CB2-18	128.71	2.50

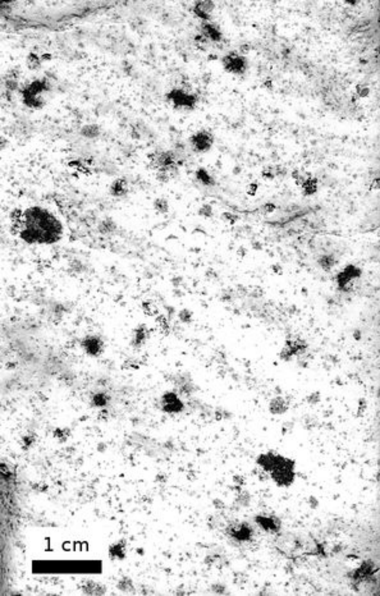
1 cm

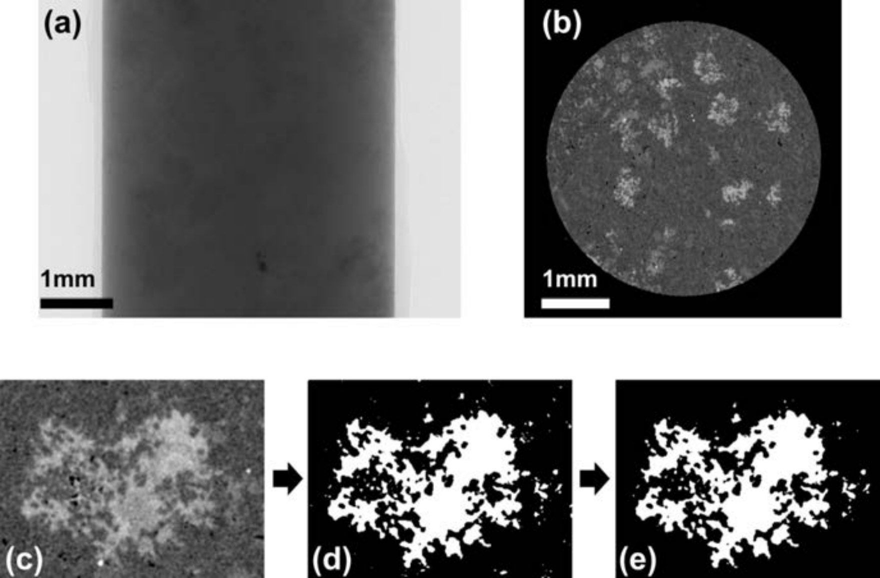
(a)
1mm
(b)
1mm
(c)
(d)
(e)

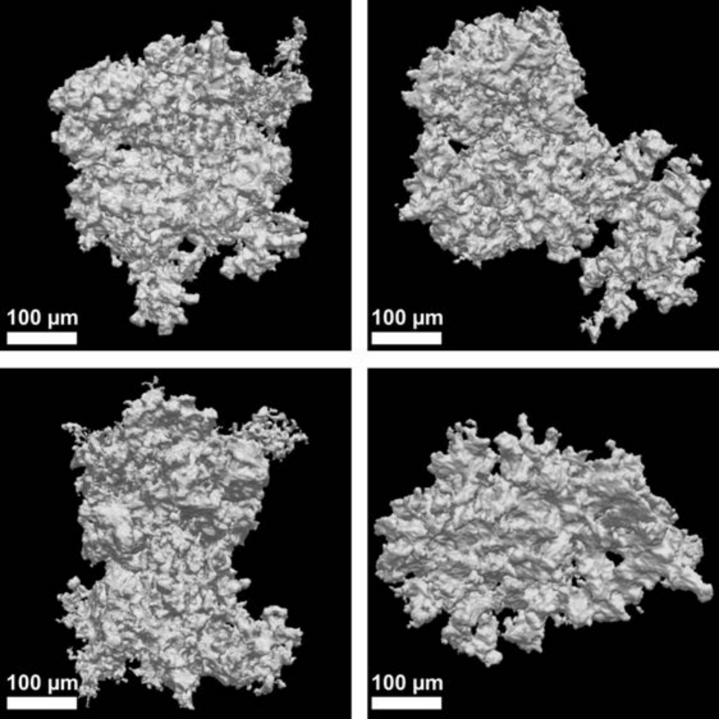
100 µm
100 µm
100 µm
100 µm

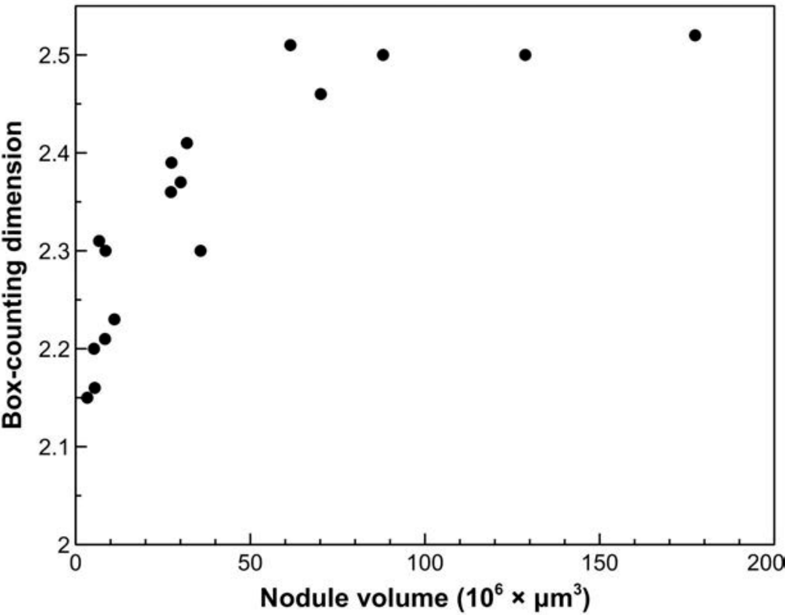
Box-counting dimension
2
2.1
2.2
2.3
2.4
2.5
0
50
100
150
200
Nodule volume ($10^6 \times \mu m^3$)

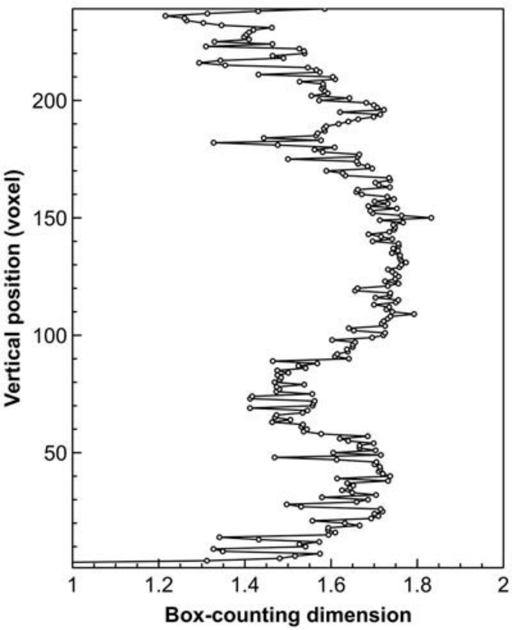

Vertical position (voxel)
200
150
100
50
1
1.2
1.4
1.6
1.8
2
Box-counting dimension

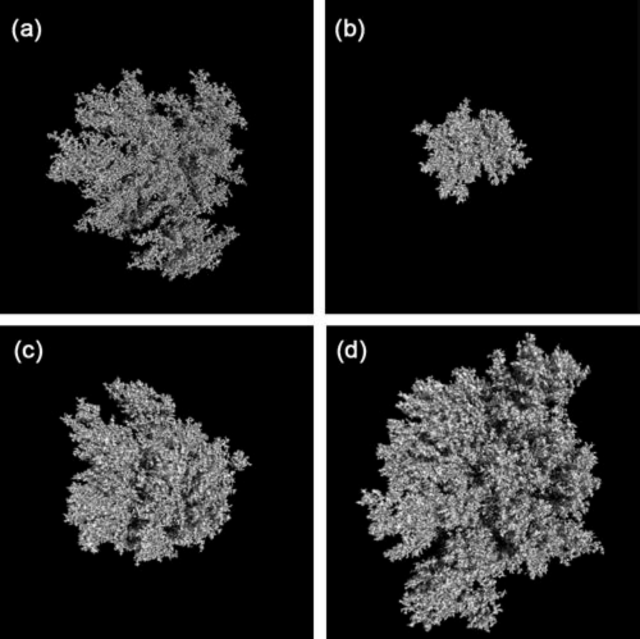
(a)
(b)
(c)
(d)

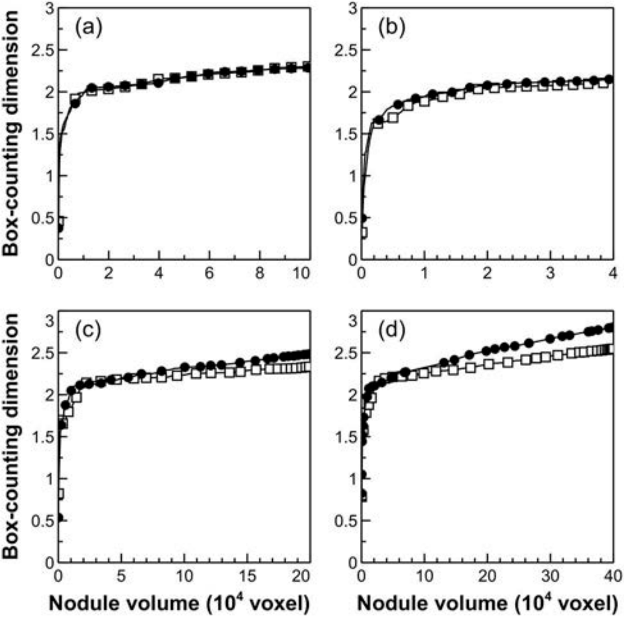
(a)
(b)
(c)
(d)
Box-counting dimension
Box-counting dimension
Nodule volume (10^4 voxel)
Nodule volume (10^4 voxel)

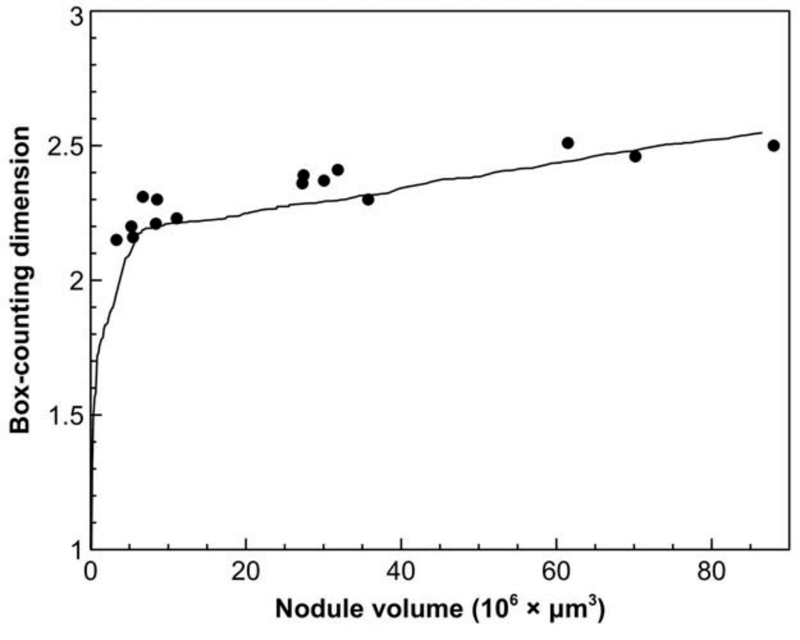

3
2.5
2
1.5
1
0
20
40
60
80
Box-counting dimension
Nodule volume (10⁶ × µm³)